Elahi-Gedwillo et al., Supplementary Figures

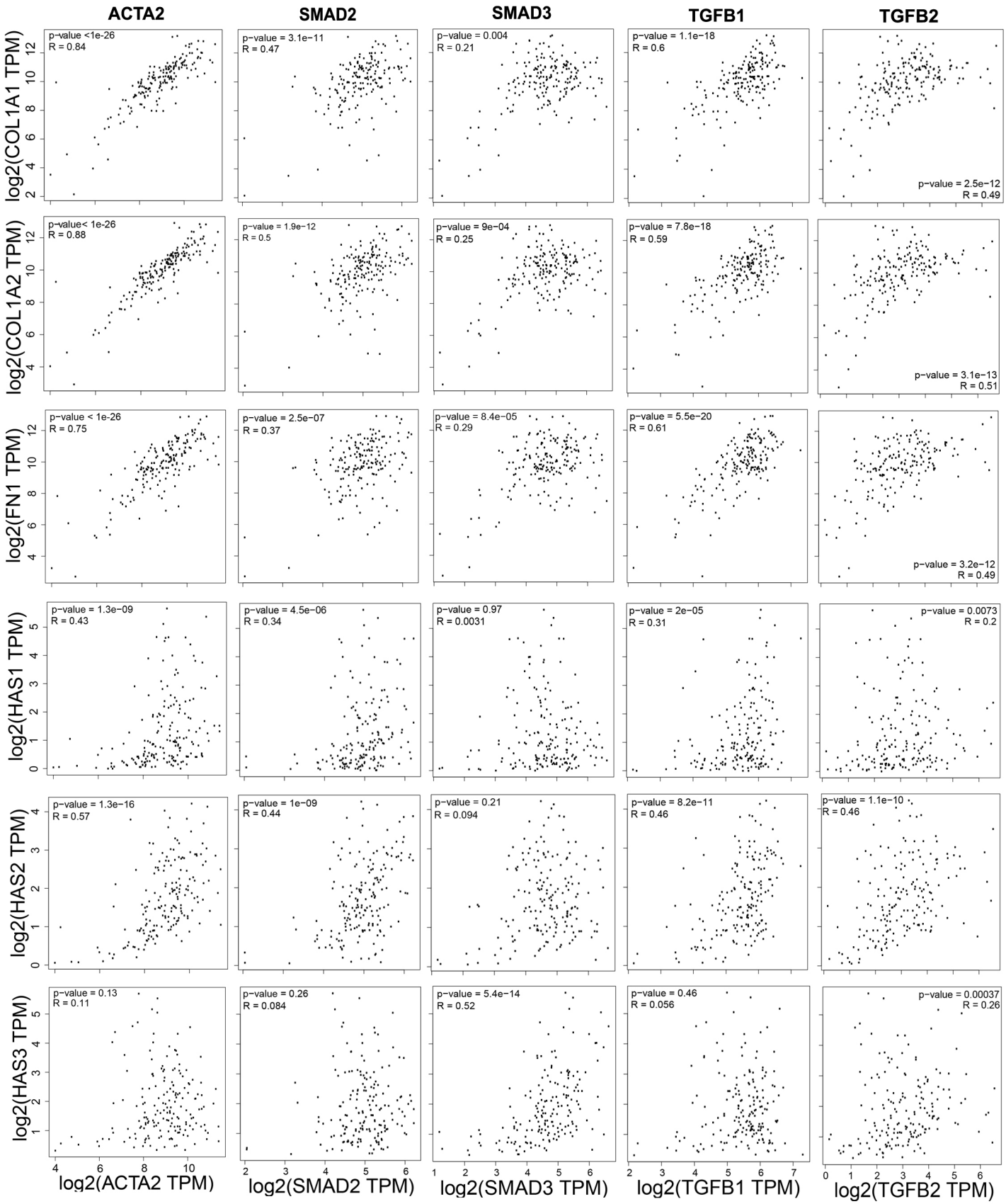

Supplementary Figure S1. Stromal ECM strongly correlates with components of the TGF-β pathway in human PDA. The TCGA human patient cohort transcriptome data (n=178) was used used here to generate scatter plots to investigate correlations in fibrosis associated genes for key stromal elements. This analysis reveals significant correlation between expression of α-SMA (*ACTA2*) and prominent ECM components commonly observed in PDA, including type I collagen, fibronectin, and hyaluronan synthases that produce hyaluronan. Consistently, significant relationships exist between TGF-β pathway transcripts and stromal ECMs. However, the strongest correlation is observed between collagen and a marker of activated fibroblasts (i.e. *ACTA2*), reflective of their significant contribution to fibrotic desmoplasia in PDA and consistent with reports of collagen being a predominant component of the dense ECM characteristically observed in the PDA stroma.

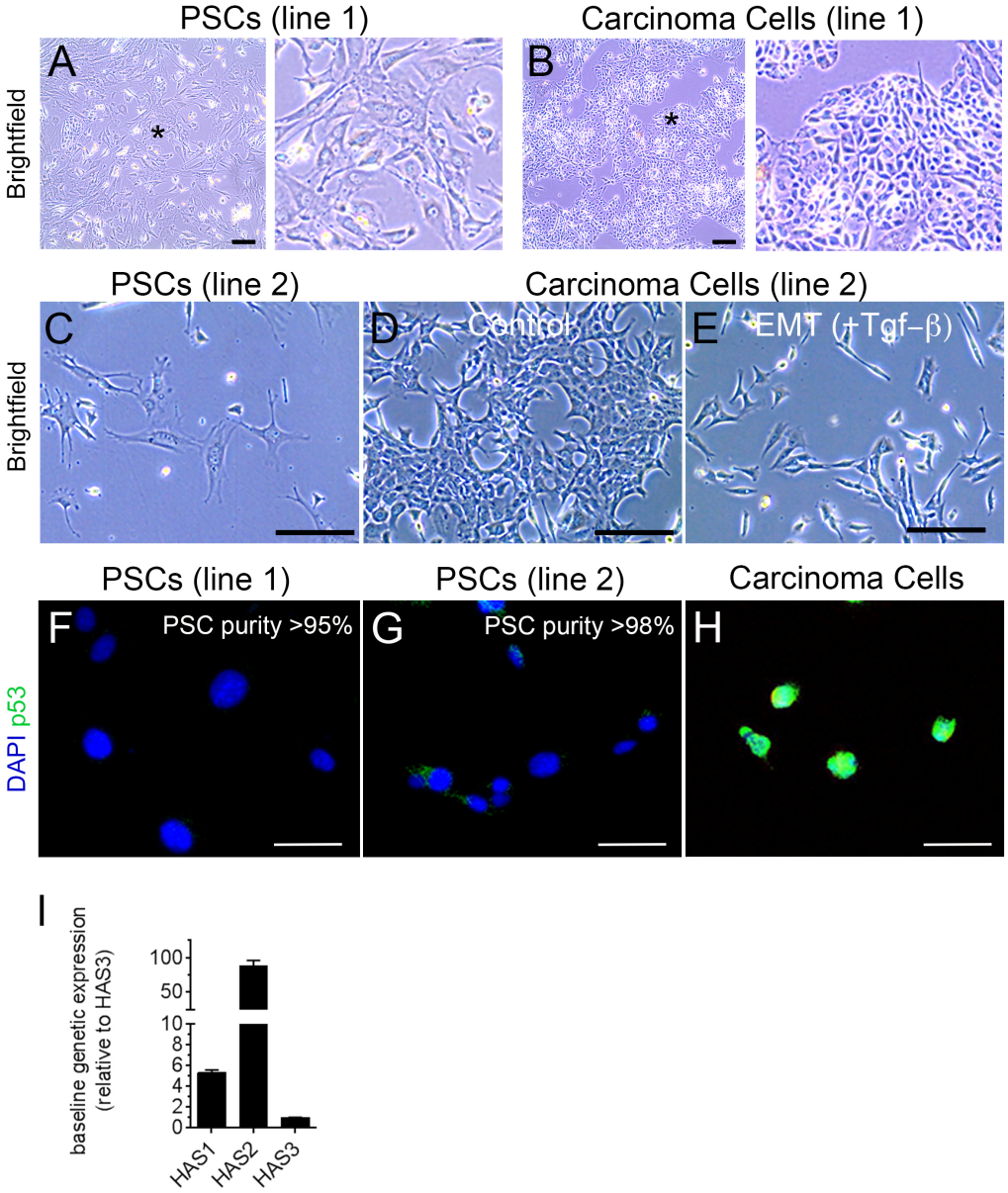

Supplementary Figure S2. PSC isolation protocol produces high purity primary cell lines. (A-E) Brightfield images illustrate the clear phenotypic differences between PSCs and carcinoma cell lines, with respective lines isolated from a common primary tumor. PSCs are generally much larger, with multiple large protrusions (**A,C**), while carcinoma cells either display classic epithelial phenotype (smaller, round, and grow in clusters, indicative of cell-cell adhesions, **B,D**) or possess a single cell phenotype (e.g. EMT phenotype, **E**). However, even single carcinoma cells are still phenotypically quite different from PSCs (**C vs. D vs. E**). (**F-H**) Immunofluorescent staining for p53, which can be used to assess purity since carcinoma cells are positive due to expression of stabilized point-mutant *Trp53* while activated PSCs (i.e. CAFs) are not. Analysis revealed >95-98% purity in early passage PSC lines (**F,G**), compared to prominent expression in primary carcinoma lines (**H**). (**I**) qPCR for Has1, 2, and 3 in PSCs. Scale bar in A-E = 100 μm, scale bar in F-H = 50 μm.

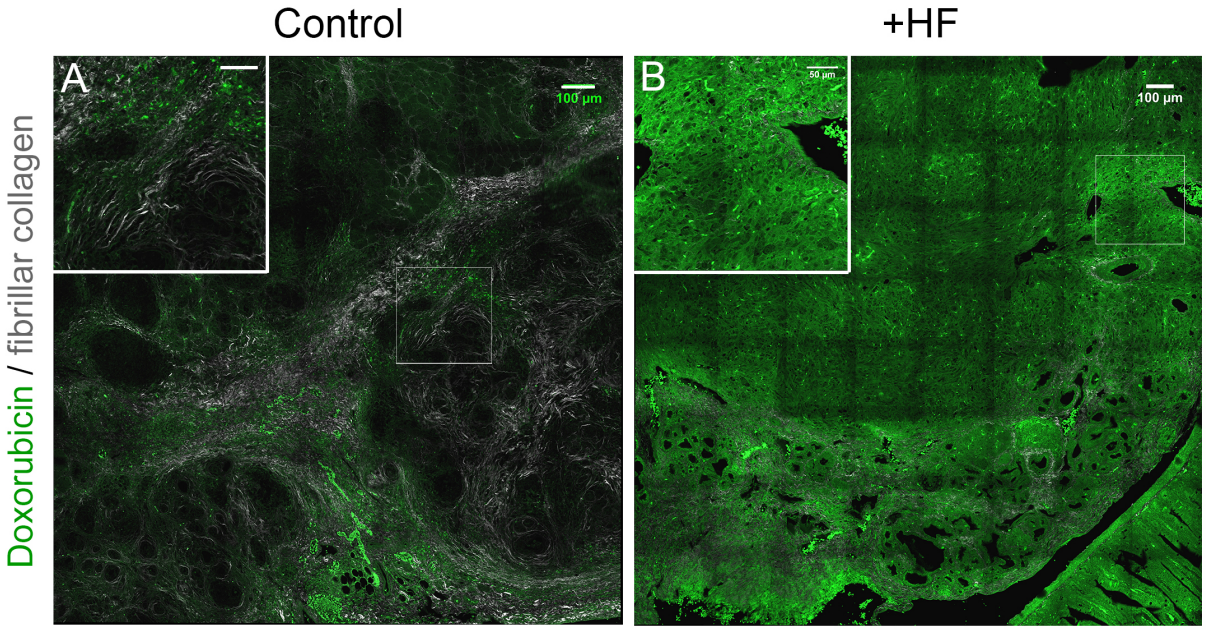

Supplementary Figure S3. Antifibrotic therapy facilitates widespread distribution of small molecule therapy. (A,B) Concomitant imaging of doxorubicin distribution (introduced i.v. 15-20 min before euthanasia to enable visualization of small molecule distribution capabilities) and second harmonic generation (SHG) imaging of fibrillar collagen reveal that small molecule perfusion capabilities negatively correlate with intratumoral fibrosis. Extensive fibrosis, as seen in untreated PDA tumors of *KPC* mice (**A**), severely limits Dox distribution, while HF-treated tumors (**B**) exhibit a significant reduction in fibrillar collagen, which facilitates restored small molecule perfusion capabilities. The images here were created by stitching together several smaller fields of view. (Scale bar in stitched images = 100 µm, scale bar in inlet images = 50 µm)

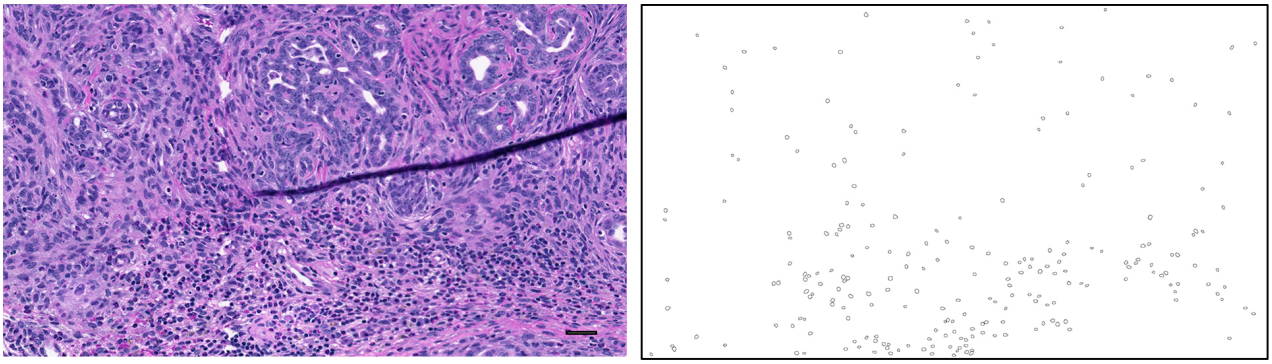

Supplementary Figure S4. Image analysis to capture histologically identifiable immune infiltrate

Quantification of immune cell populations in H&E stains was performed using an algorithm to detect histologic immune infiltrate by filtering nuclei on the basis of size, shape, and density. To estimate immune infiltrate in H&E sections, the quantitative image-processing algorithm was created in FIJI, where a built-in color deconvolution plugin was used to separate the H&E color channels and isolate the nuclei. Immune cells were distinguished by thresholding for specific nuclear characteristics (immune cells were presumed to have very small, round, and dark nuclei). The algorithm selected for nuclei that were smaller than the comparably larger nuclei of carcinoma cells, but larger than random debris, with circularity set to 0.75-1.00 to filter out the elongated nuclei of fibroblasts. Nuclear size parameters were determined by iterating the pixel range until the maximum particle size was small enough to exclude the visibly larger nuclei of carcinoma cells, and the minimum was small enough to exclude random debris.

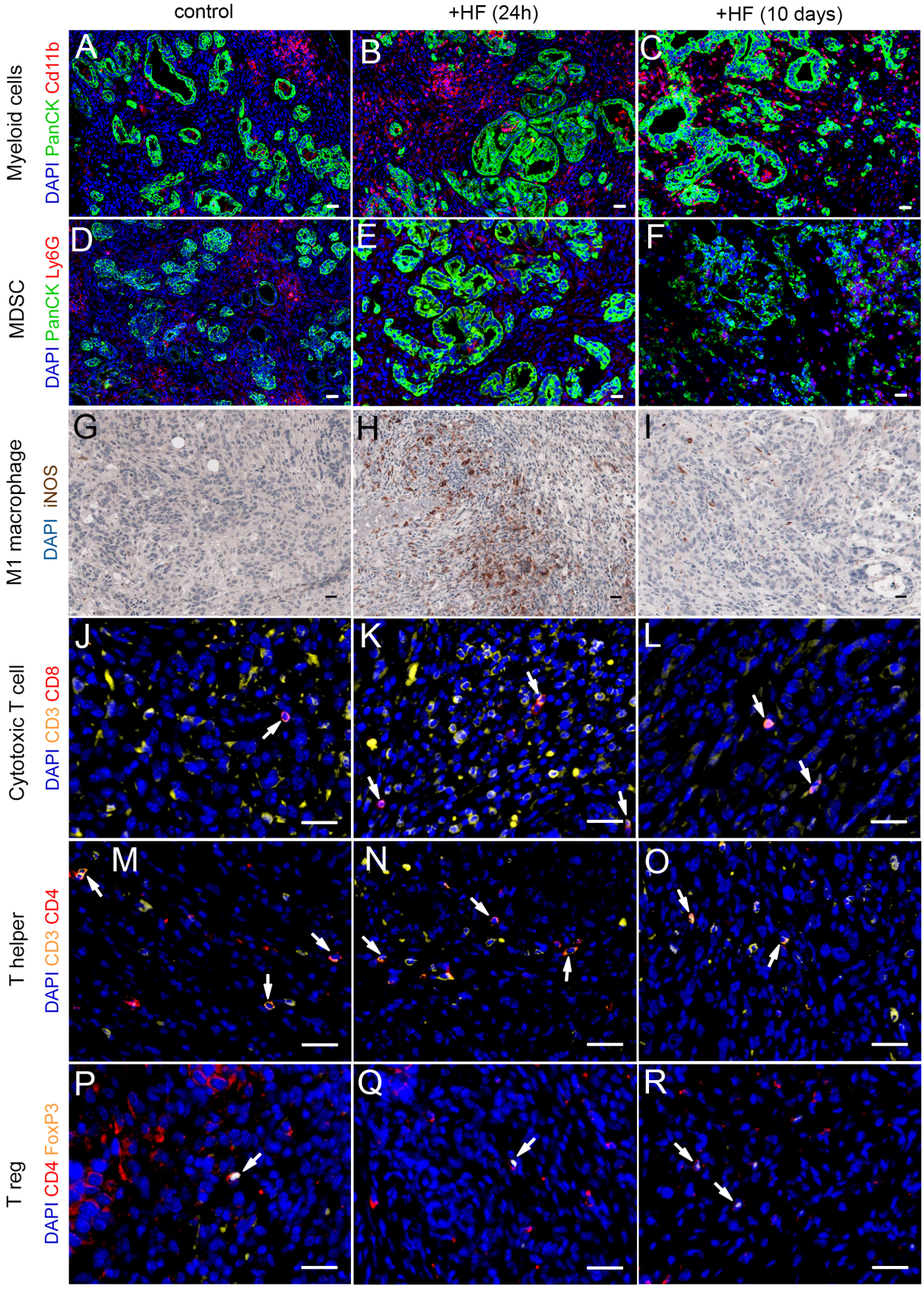
control
+HF (24h)
+HF (10 days)
Myeloid cells
DAPI PanCK Cd11b
MDSC
DAPI PanCK Ly6G
M1 macrophage
DAPI iNOS
Cytotoxic T cell
DAPI CD3 CD8
T helper
DAPI CD3 CD4
T reg
DAPI CD4 FoxP3
A
B
C
D
E
F
G
H
I
J
K
L
M
N
O
P
Q
R

Supplementary Figure S5. Immunofluorescent (IF) and immunohistochemistry (IHC) staining of HF-induced modulation of the immune landscape. (**A-C**) IF staining for Cd11b (red) indicates the presence and localization of myeloid cells in relation to carcinoma cells (PanCK, green) across different treatment groups, indicating a significant increase in overall number and distribution 24 hours after HF (**B**), and an apparent sustained improvement in distribution in mice treated with HF for 10 days (**C**). (**D-F**) IF staining for Ly6G (red), a marker commonly used to identify MDSCs, was performed to define localization among cancer cells (PanCK, green), and determine if this cell population explained the influx of Cd11b+ cells. Data show no significant difference across treatment groups. (**G-I**) IHC staining for iNOS, a marker commonly used for “M1” classically activated inflammatory macrophages, was performed, revealing a significant increase 24 hours and 10d after HF treatment (**H,I**). (**J-R**) Tri-color IF staining was performed for multiple T cell populations. (**J-L**) To identify cytotoxic T cells, staining for DAPI (blue), CD3 (yellow), and CD8 (red) was performed. This revealed a significant increase in the number and distribution of cytotoxic T cells 24 hours after HF administration (**K**). (**M-O**) To identify T helper cells, staining for DAPI (blue), CD3 (yellow), and CD4 (red) was performed. Data indicated no difference between treatment groups. (**P-R**) To identify T regulatory cells, staining for DAPI (blue), CD4 (red), and FoxP3 (yellow) was performed. This revealed no significant difference between treatment groups. (Scale bar = 25 μm, arrows indicate T cells that express all three respective IF markers, denoting a positive cell)

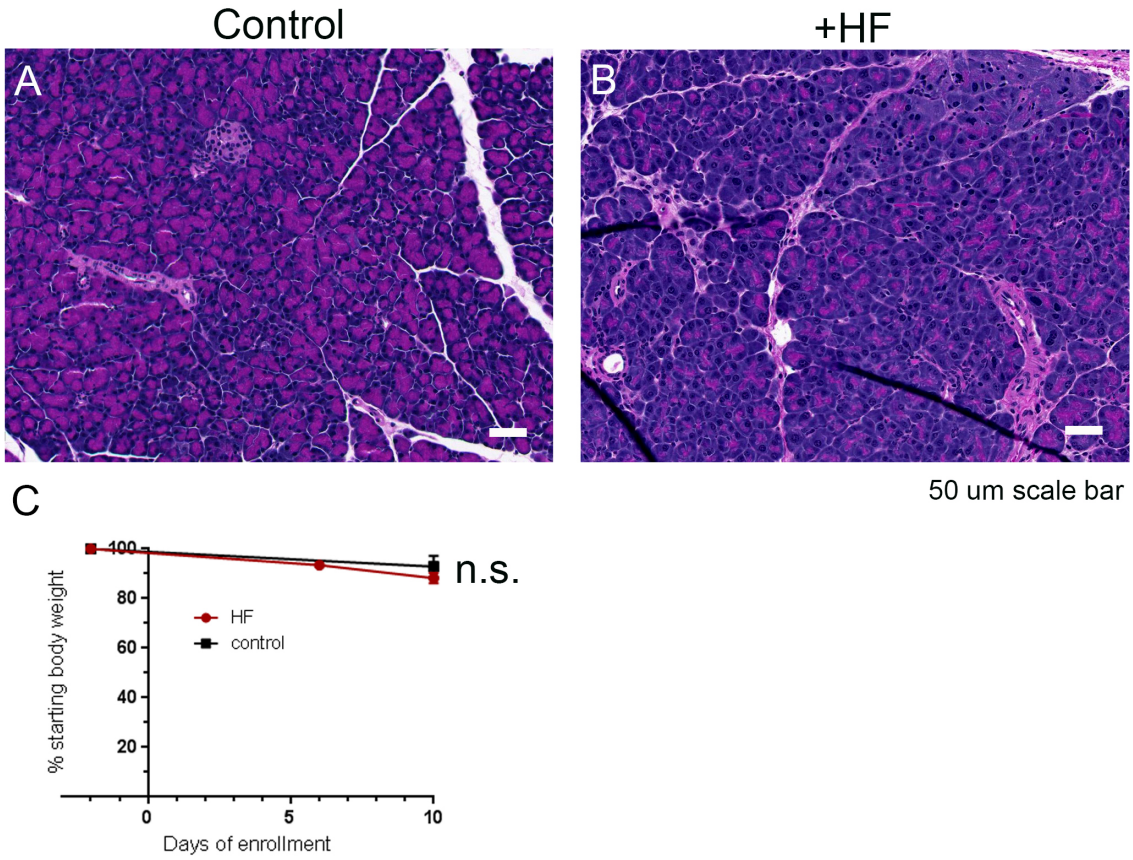

Supplementary Figure S6. Normal adjacent pancreas appears histologically normal. Examination of H&E sections from normal-adjacent regions do not display signs of necrosis found in tumors. Furthermore, there was no significant difference in body weight over the course of the study.